EXPERIMENTS AND MODELLING OF RODUCER GAS BASED RECIPROCATING ENGINES

G. Sridhar[1], P.J. Paul[2] and H.S. Mukunda[2]

Combustion, Gasification and Propulsion Laboratory
Department of Aerospace Engineering
Indian Institute of Science, Bangalore 560 012, India.
1 Research student 2 Faculty

ABSTRACT

A 20 kW reciprocating engine is operated using producer gas derived from a modern open top downdraft re-burn biomass gasifier that has been evaluated by rigorous laboratory performance testing over several hundred hours. The engine is operated at varying compression ratio (CR) from 11.5 to 17.0 and ignition timings from 30 to 6° before Top Centre (TC). The engine – alternator system is characterised for its performance by the simultaneous measurement of gas and airflow rates, gas composition (online), emission levels and power delivered. It is also instrumented to obtain the in-cylinder behaviour in the form of pressure-crank angle (p - θ) diagram to assess the thermodynamic behaviour of the engine.

Three-dimensional (3-D) simulation of the flow field in the combustion chamber (involving piston-bowl arrangement) through the cycle up to the start of the combustion is used to obtain inputs on the turbulence intensity (u') and length scale (l_T) for the modeling of the flame propagation process in a zero-dimensional model (0-D) designed to predict the p – θ curve. The flame propagation and heat release processes make use of eddy entrainment and laminar burn-up model. The data on u' extracted from the 3-D flow calculations match reasonably well with experiments till compression stroke but are in contradiction with trends close to TC. This is reasoned to be due to limitation of the k-ε model to capture transient effects due to reverse squish phenomenon.

The 0-D model took into account the experimental behavior of the u' in the post-TC period to attempt to match the observed p - θ data over a range of CRs and ignition timing advances. While these predictions match well with the experimental data at advanced ignition timing at both higher and lower CRs, the peak pressure is under-predicted at lower ignition advances; reason are traced to increase in flame area and propagation speed due to reverse squish effect. When these are accounted in the model, the p - θ curves are predicted better.

INTRODUCTION

With the renewed interest in green energy, biomass based technologies are becoming major players in the field of power generation. Gasification is one such process where clean gas could be generated and used as a fuel gas in internal combustion engines. These could either be used in standard diesel engines in dual-fuel mode or gas alone in spark-ignited engines. There has been very little scientific work done using producer gas in reciprocating engines, however there is a large body of work on natural gas based engines both in terms of experimental work as well as modeling [1]. Work in the field of producer gas engines has received lesser attention primarily due to non-availability of standard gasification system that could produce consistent gas both in terms of composition and quality.

Work related to biomass gasification and its use in reciprocating engines has been extensively carried at Combustion Gasification and Propulsion Laboratory in the last two decades and this has resulted in world class gasification technology. The system has undergone extensive testing both at the laboratory and field level and likewise in India and overseas. The current work is in continuation of range of studies aimed at laying the scientific foundations for the development of biomass based gasification technologies [2 – 5] aimed at power generation in combined heat and power

mode as well as high grade heat for specific applications. The principal elements of the biomass gasification technology are the reactor, cooling and cleaning system. The reactor is designed to generate a gas that captures as much of the energy in the biomass as possible and with very little tar. The cold gaseous fuel so obtained has a composition of $CO \sim 18 – 20$ %, $H_2 \sim 18 - 20$ %, $CH_4 \sim 1 - 2$ %, $CO_2 \sim 10 - 12$ %, $H_2O \sim 2.5$ % and $N_2 \sim$ rest with casuarina wood pieces used for the present study.

This work is a continuation of the earlier work of the authors [3]. The present paper is devoted to modeling aspects and makes use of the experimental results from the earlier work [3] for comparing against the 0-D predictions. One of the most interesting features of the experimental work is that the gas engine converted from a diesel engine at CR of 17, ran on producer gas fuel (with the nominal composition as indicated above) without any limitation due to knock even though some of the earlier workers had experienced knock with charcoal based producer gas [6]. The current paper reports a 0-D thermodynamic model, which has been constructed with inputs from 3-D CFD calculations particularly for the turbulent flame propagation. The selective good comparison of p - θ curves at advanced ignition timings and the under-prediction at retarded ignition timings irrespective of the CR are discussed and the issues regarding the current gaps in modeling are brought out.

NOMENCLATURE

$f A$	Spherical flame area, m2
$l A$	Laminar burning area, m2
CA	Crank Angle
$l T$	Integral Length/Characteristic length, m
$b m$	Mass of mixture burned, kg
MBT	Maximum Best Torque
P0	Initial pressure, kPa
P	Motoring pressure, kPa
$l S$	Laminar burning velocity, m s-1
TC	Top Centre
p - θ	Pressure-Crank angle
POP	Point of peak Pressure
RSF	Reverse Squish Flame
u	Turbulent intensity, m s-1
$T u$	Characteristic speed, m s-1
$u \rho$	Unburned gas density, kg m –3

μ	Parametric mass, kg
$b \tau$	Characteristic time, sec
Φ	Fuel equivalence ratio
α	Recycled gas fraction
0-D	Zero dimensional
3-D	Three dimensional

THE EXPERIMENTAL DETAILS

A systematic scientific investigation has been conducted on a multi-cylinder gas engine at varying CR of 17, 14.5, 13.5 and 11.5 using producer gas fuel. The engine utilized for the study is a convert of a production diesel engine, having the same cylinder and piston of the compression ignition engine. The salient feature of the experimental engine is shown in Table 1. The relevant parameters like the gas and air flow rates, gas composition, power delivered and exhaust emissions were continuously monitored. The in-cylinder p - θ data was obtained using a pre-calibrated Piezo based pressure transducer (PCB make) in steps of one crank angle (CA). M/s PCB make piezo sensor Model No. HS 111A22 with built-in charge amplifier, having a resolution of 0.69 kpa, rise time of 1 micro-second and discharge time constant of more than 500 second, was used for pressure measurements. The sensor was connected to the combustion chamber using a passageway of 1 mm diameter and 40 mm in length in the cylinder head. Due to the above mounting arrangement, there is a possibility of phase lag between the cylinder pressure and transducer output to an extent of 0.4 degree CA. This point need to considered while interpreting the results.

The trace showed smooth combustion behaviour even at the highest CR of 17 without any sign of knock even at advanced ignition setting. The engine delivered a peak shaft power of 20 kW (@ 1500 rev/min), with the Maximum Best Torque (MBT) timing between 6 and 10° CA at CR of 17 and reduced to 17.6 kW at a MBT about 16° CA at a CR of 11.5. The reduction in power is about 2.2% per unit decrement in CR and this is well with in the range of 1 to 3% gains per unit incremental of CR [7]. This interesting feature of low ignition advance is due to burning velocity of producer gas being higher by about 30 % than natural gas at the engine operating conditions. This inference is based on the experimental

evidence available from the literature [1], which indicates that the MBT for natural gas (94% methane) is about 15 °CA at CR of 14.3 as against 10° CA with producer gas [3] with engines of similar combustion chamber geometry.

THE 0-D MODEL

The model comprises of sub-models to simulate the four processes of an engine cycle namely, intake, compression, heat release followed by expansion and exhaust. The various sub-models used in the above simulation are (a) the filling and emptying technique for intake and exhaust processes as outlined in Heywood [7], (b) Eddy Entrainment and Laminar Burn-up (EELB) model for simulation of heat release as derived by Keck [8] and (c) the heat loss due to convection based on Annand's convective heat transfer correlations as discussed by Baruah [9]. It has been established by earlier researchers that flame propagates in a laminar mode till the flame kernel attains a critical size, beyond which the propagation becomes turbulent [7, 10]. In one case, Khalagati [10] has identified the critical size of the flame to be around 11 mm radius for the propane and air gas mixture. This delay period is also considered as the time in which 1 to 10% of the initial unburned mass is consumed [7]. The flame propagation (or heat release) is modelled as a two-zone model, where a thin wrinkled multi-connected laminar flame separates the burned and the unburned mixture. The EELB model as formulated by Keck [8] is represented by two equations namely,

$$\frac{dm_b}{dt} = \rho_u A_f S_l + \frac{\mu}{\tau_b} \qquad (1)$$

$$\frac{d\mu}{dt} = \rho_u A_f u_T - \frac{\mu}{\tau_b} \qquad (2)$$

Where $\mu = \rho_u l_T (A_l - A_f)$. Equation 1 represents the mass burn rate, whereas Eq. 2 represents the rate of change of unburned mixture within the flame front. In these equations, there are two quantities, namely the characteristic speed and length, which could be related to the turbulence parameters namely u and l_T as identified in Heywood [7]. Therefore, the task reduces to that of determining u and l_T, which are found using empirical correlations or from fundamental studies. The second approach is chosen here and for this purpose, CFD analysis is conducted to obtain u and l_T.

Laminar burning velocity is another input parameter required for the heat release model. It is computed using an inhouse code called 'FLAME CODE' [4] that uses a transient calculation procedure to extract the properties of one dimensional laminar premixed flame. The code has been validated with experimental results at ambient pressure and initial temperatures [4,11]. The fuel considered was of nominal composition with 20 % each of H_2 and CO, 2% CH_4, 12% CO_2 and rest N_2. Theoretical burning velocity calculation has been done at varying equivalence ratio, initial temperature and pressure and with *varying amounts of recycled gas ranging from 0 to 10%.* An expression derived from this analysis for fuel-air equivalence ratio between 0.9 to 1.3 is as given below

$$S_l \ (m/s) = 0.95 \left(\frac{P}{P_0}\right)^{0.2744} (1 + 1.21(\phi - 1))(1 - 2.4\alpha) \quad (3)$$

Where φ is equivalence ratio and α is the recycled gas mass fraction. The burning velocity dependence upon the initial temperature is built into the motoring pressure term in Eq. 3. The burning velocity is about 30 % higher than for natural gas; it is quite sensitive to the variations in H_2 and CO content that may occur naturally in the gasification process. A sensitivity analysis of variation in CO and H_2 content towards laminar burning velocity at an equivalence ratio of about 0.9 revealed the burning velocity reduction by about 7% for every 1% reduction in H_2 or CO content.

CFD CALCULATIONS

A number of researchers [12-16] have worked on 3-D computational studies with respect to the fluid flow in engine cylinder, simulating the motored or non-fired condition. Majority of the studies address geometries formed by a moving piston, either flat [12] or bowl [13], and without or with moving intake valve [12, 14]. The earlier computational results [12-14] compare well with single point experimental

measurements obtained using hot wire anemometry, LDV or PIV. Studies on bowl-in piston geometry [16] reveal higher turbulence levels as compared to the flat piston geometry due to enhanced swirl and squish effect. Experimental studies involving bowl geometries with re-entrant design by Corcione et al [17] and Cantania et al [18] exhibit increase in turbulence kinetic energy (k) during post - TC as against declining trend [19] in case of simple bowl piston design. This is inferred as due to higher shear zones with re-entrant geometries [17].

Most of these simulations have been carried out using standard k-ε [12, 14-16] or RNG k-ε [13] turbulence model with and without the compressibility effect due to density variation. In the cases where the compressibility effect is accounted for, there is no definiteness on the choice of the constant for velocity dilatation term [13,15] and it varies from +1.7 to –1.0. As it is not simple to validate turbulence model in engine like situation, there is even less certainty on the contribution of velocity dilatation term to the turbulence dissipation rate. The ability of k-ε model in predicting turbulence quantities under engine like conditions has been examined by Lebrere et al [20] by comparing with higher order Reynolds stress model on simple flat piston geometry. The Reynolds stress model predicts the presence of anisotropy during compression, a feature argued to be the reason for higher u' values with k-ε model (~ 20% higher). The present results from k- ε model when compared with experiments confirm this observation.

A 3-D CFD analysis has been conducted here on the engine combustion chamber geometry with a flat cylinder head and hemispheric bowl-in piston. The geometry replicates the gas engine measuring 110 mm bore and 116 mm stroke with a bowl volume of 56 cc. The bumping clearance at 17 CR is 1.5 mm and increases to 5.0 mm at 11.5 CR. The geometry also comprises of a moving intake valve (non-swirl type) and a moving piston to simulate the fluid flow into and out of the cylinder. The geometry is fitted with a body fitted grid, with pressure boundary condition imposed at the intake valve to allow flow into or out of the flow domain. The physical values applied as the boundary condition have been derived from the actual pressure measurements in the intake manifold,

close to the intake valve. This is consistent with some of the earlier studies with moving intake valve [14]. Similarly, simulation of valve movement has been based on valve lift measurements on the engine. The opening and closing of the intake valve are in accordance with the actual valve timing of 26° before TC and 66° after TC respectively. The initial condition in the flow domain is based on 0-D motored results. The computations have been carried out using a commercial CFD code called CFX4.3 on a Pentium personal computer. The CFD code solves the 3-D, ensemble-averaged Navier-Stokes and enthalpy equations governing turbulence and compressible gas flow along with heat transfer for a geometry involving a moving grid to simulate the valve and piston movement. The algorithm employed for spatial and temporal discretisation is 1st order accurate hybrid and backward difference schemes respectively. To resolve the turbulence parameters, standard k-ε model has been chosen without and with compressibility effects due to velocity dilatation. The working fluid is treated as a single gas since combustion is not simulated.

The computations have been carried out to simulate engine operation at 1500 rev/min, with time step of the order of 0.5 CA (50 µs). Calculations have been made with the number of cells in the flow domain at 0.1 and 0.2 million cells. The grid and time step independence of the calculations have been verified by using the finer grid results. The principal results of direct use from the calculations are u' and the corresponding l_T. the grid arrangement with the piston at bottom centre and the intake valve open is shown in Fig. 1.

CFD RESULTS

The results of the CFD analysis have been compared with experimental results of an available engine of similar configuration conducted by Cantania et al [18]. The Laser Doppler Velocimetry (LDV) results belong to a diesel engine with a cylindrical, slightly re-entrant bowl at CR of 18:1 operating at varying speeds. Figure 2 shows the comparison of the experimental [18] u' (over all the range of frequencies consistent with k- ε formulation) with CA at 1500 and 2000 rev/min (mean piston speed of 4.3 and 5.8 m/s respectively) with computed values at a speed of 1500 rev/min

(mean piston speed of 5.8 m/s). The comparison of the u' between the two results appears fair (considering the fact that the geometries are similar, but not identical) till about inlet valve closure; beyond this point, however, one finds opposing trends in the variation of the u' with CA. As the piston starts compressing the fluid, there is an increase in u' and peaks at 330° CA beyond which there is a decline in u' as against continuous decline in the measured values. In the post-TC region, there is again a contradictory trend in comparison to experimental results. This feature is unaltered even when compressibility effect is accounted for by choosing a constant of -0.373 [15] for the velocity dilatation term in the ε-equation. In the work of Han et al [13], using RNG k-ε model on Mexican hat piston top where the effect of velocity dilatation and kinematic viscosity are accounted in the ε equation, similar qualitative behaviour in u' has been observed as noted here.

Experimental studies strongly suggest the trend of increase in u' with re-entrant bowl-in piston configuration compared to simpler bowl-in piston configuration in the post-TC period [17]. If one were to assume the existence of a behaviour similar to experiments in the post-TC period with 0-D model (as shown later), the heat release rate behaviour is predicted correctly. It appears therefore that the turbulence model does not capture sharp transients in CFD calculations in the post-TC period and capturing these effects needs a reexamination of the turbulence model.

Figure 3 containing the variation of u' with CA indicates that the u' variations are independent of CR; these are consistent with earlier observations [21, 22]. The l_T calculated using k and ε are also shown in Fig. 3 indicates that lT is higher at lower CR compared to higher CR and qualitatively consistent with the experimental results [22].

The CFD studies reveal significant spatial variations of u' and lT within the cylinder. However, single point values have been taken at location about a third of the bowl radius from the cylinder axis and used in 0-D calculation. This single point value is an average representative of large portion of the cylinder. This is clear from the contour plots for k in Fig 4, which shows fairly uniform high intensity in the core of the bowl and decreasing intensity in the region close to the walls.

0-D MODELLING RESULTS

The sub-models of the 0-D model other than the heat release model are validated initially by comparing with the experimental *motoring* p - θ curves. The primary information required to initiate the heat release effect is the ignition delay period that is estimated by superimposing the motoring curve over the experimental firing curve and taking the point of deviation from the point of ignition as the delay period. During the ignition delay period, about 1% of the initial mass is assumed to have consumed [7], corresponding to a flame kernel of about 12 mm radius. The flame is assumed to move into the bowl during kernel formation; the dislodging of the flame from its point of ignition is well identified by Keck [8].

Principal features of the results are presented in Table 2. This table describes the results of 0-D predictions using u' values obtained from CFD studies and experimental results on an engine with similar configuration [18]. The propagation speeds both inside and outside the bowl during the course of flame propagation and their influence on the p - θ predictions are given. The predictions on p - θ at both CRs (Case I – III) compare excellently with the experimental data. One such result (Case I) for CR=17 at 26° CA is shown in Fig. 5. These predictions are made by considering spherical flame both inside and outside the bowl and u' (post-TC) based on experimental trend [18]. The Point of peak Pressure (POP) also coincides excellently in Cases I to III. With different u' trends (post-TC as in Fig. 2), the prediction match well for Case I with CFD trend as indicated in the inset (no .2) of Fig. 5 and marginally under-predicts with experimental trend [18] as shown in the inset (no. 3) of Fig. 5.

The prediction for Case IV (CR=17) at 17° CA advance is lower with the same considerations as above. A careful analysis of experimental p - θ curve reveals sharp increase in the cylinder pressure during the later stages of combustion and this seems to coincide with the onset of significant reverse squish. The flow field during the peak of the reverse squish phenomenon is as presented in Fig. 6, shows the flow vectors

directed outwards. Further, gas velocity behaviour in this zone calculated using the correlation given in Heywood [7] is shown in Fig. 7. In the presence of combustion, these gas velocities are known to be larger by a factor of two as observed experimentally [23]. Taking these into account, a hypothesis has been made for flame propagation beyond the bowl region: the flame penetrates the flat section at the top with velocities as in Fig 6C and then moves in an annular cylindrical manner from the cylinder head downwards. With this Reverse Squish Flame (RSF) hypothesis, the prediction for Case IV matches well (shown in Fig. 8), except for POP occurring about 1° CA earlier.

The prediction for Case V (CR=11.5) matches experimental p - θ, but the peak pressure is under-predicted with spherical flame assumption and over-predicted with RSF hypothesis. With squish velocities being lower at CR=11.5, RSF hypothesis may not be completely valid calling for a specific re-examination.

For Case VI (CR=17) at 12° CA, the results are largely under–predicted with spherical flame assumption. The underprediction is to a lesser extent with RSF hypothesis as shown in the inset (no. 1) of Fig. 8 with POP occurring 1° CA earlier. The only reason for this short fall is the under estimation of the energy in the gas. When higher percentage of methane (4%) is accounted, the prediction improves substantially and this is shown as inset (no. 4) of Fig. 8. With different U trends, the predictions (Case VI) match reasonably well except for under-prediction of peak pressure with experimental trend [18] as shown in the inset (no. 2) of Fig. 8. Where as, there is gross under-prediction with CFD trend as shown in the inset (no. 3) of Fig. 8.

The above analyses reaffirms that U has a major role to play in heat release rate; this is particularly true at retarded ignition setting where major part of the combustion occurs during reverse squish regime. With k-ε formulation unable to capture the U trend correctly, the choice of U behaviour post-TC based on experimental observation [18] has been proved to be correct.

CONCLUSIONS

This paper has reported a study on producer gas reciprocating engines; experiment at CR of 17 has shown knock free performance with producer gas fuel. CFD studies indicate qualitative behaviour of U from the initiation of intake valve opening till mid-way of compression stroke, beyond which there is contradictory trend not captured by k-ε model. Use of U and lT values from the CFD studies and experiment [18] in 0-D modelling predicted the p-θ curves quite accurately at larger ignition advance and at all CRs. However, the prediction deviates from the experimental values at high CRs and retarded ignition timing, where reverse squish phenomenon has a significant role in modifying the mass burn rate. The results are predicted better when this effect is accounted in the model.

The choice of the ignition timing for producer gas is such that major part of the combustion occurs during reverse squish period and therefore the study of the influence of this phenomenon becomes relevant. This study has therefore uncovered the role of reverse squish regime in enhancing/retarding burn rate in gas engine combustion, which hitherto has not been addressed. This study clearly identifies the problems of traditional 0-D model when major part of the combustion occurs during reverse squish regime in bowl-in piston combustion chamber geometries. This therefore brings out the need the further examination of 0-D modelling.

REFERENCES

1. Stone C.R., Mendis K.J.S. and Daragheh M., 1996, "Measurements and modelling of a lean burn gas engine", Proceedings, Institution of Mechanical Engineers. , 210, pp. 449-462.

2. Mukunda H.S., Dasappa S. and Shrinivasa U., 1993, "Open-top wood gasifiers", Renewable Energy –Sources for fuels and electricity, Island press, Washington, p. 699-728.

3. Sridhar G., Paul P.J. and Mukunda H.S., 2001, "Biomass derived producer gas as a reciprocating engine fuel-an experimental analysis", Biomass & Bioenergy, 21, pp. 61-72

4. Mishra D.P., Paul P.J. and Mukunda H.S., 1994, "Computational studies on the flame propagation in producer gas-air mixture and experimental comparisons", Proceedings, 13th National conference on IC engines and Combustion, Bangalore, pp. 256- 262.

5. Dasappa S., Paul P.J., Mukunda H.S. and Shrinivasa U., 1998, "Wood-char gasification: Experiments and analysis on single particle and packed beds", Proceedings, 21st symposium (international) on combustion, The Combustion Institute, Pittsburgh, pp. 1335-1342.

6. Martin J. and Wauters P., 1981, "Performance of charcoal gas internal combustion engines", Proceedings, International conference – New energy conversion technologies and their commercialization, Vol 2, pp. 1415-1424.

7. Heywood J.B., 1989, Internal combustion engine fundamentals, International edition, McGraw-Hill Book Company, New York.

8. Keck C.J., 1982, "Turbulent flame structure and speed in spark ignition engines", Proceedings, 19th Symposium (international) on combustion, The Combustion Institute, Pittsburgh, pp. 1451-1466.

9. Baruah P.C., 1986, "Combustion and cycle calculations in spark ignition engines", In the thermodynamics and gas dynamics of internal combustion engines Ed: Horlock., J.H., and Winterbone, D.E., Oxford science publication, pp. 823-865.

10. Kalghatgi T.G., 1985, "Early flame development in a spark-ignition engine", Combustion and Flame, 60, pp. 299-308.

11. Chakravarthy P., Mishra D.P., Paul P.J. and Mukunda H.S., 1993, "The theoretical calculations of the limits of flame propagation for producer gas mixture", Proceedings, 4th National meet on biomass gasification and combustion, pp. 28-37.

12. Reuss D.L., Kuo T.W., Khalighi B., Haworth D. and Rosalik M., 1995, "Particle image velocimetry measurements in a high-swirl engine used for evaluation of computational fluid dynamics calculations", SAE paper 952381, pp. 2073-2092.

13. Han, Z., and Reitz, R.D., 1995, "Turbulence modeling of internal combustion engines using RNG k-ε model", Combustion Science and Technology, 106, pp. 267-295.

14. Jones P. and Junda J.S., 1995, "Full cycle computational fluid dynamics calculations in a motored four valve pent roof combustion chamber and comparison with experiments", SAE paper 950286, pp. 595 - 610.

15. Jennings M.J., 1992, "Multi-dimensional modeling of turbulent pre-mised charge combustion", SAE paper 920589, pp. 1106 - 1124.

16. Schapertons H., and Thiele F., 1986, "Three dimensional computations for flow fields in DI piston bowls", SAE paper 860463, 1986, pp. 135-151.

17. Corcione F.E. and Valentino G., 1994, "Analysis of in-cylinder flow processes by LDA", Combustion and Flame, 99, pp. 387-394.

18. Cantania A. E. and Spessa E., 1996, "Speed dependence of turbulence properties in a high-squish automotive engine combustion system", SAE paper 960268, pp.313-334.

19. Brandl F., Reverencic I. and Carterllieri, W., 1979, "Turbulent air flow in the combustion bowl of a D.I. diesel engine and its effect on engine performance", SAE paper 790040, pp.172-199.

20. Lebrere L. and Dillies B., 1996, "Engine flow calculations using a Reynolds stress model in the Kiva-II code "SAE paper 960636, pp. 882-904.

21. Lancaster D.R., 1976, "Effects of engine variables on turbulence in a spark-ignition engine", SAE paper 760159, pp. 671-688.

22. Ikegami M., Shioji M. and Nishimoto K., 1987, "Turbulence intensity and spatial integral scale during compression and expansion strokes in a fourcycle reciprocating engine", SAE paper 870372, pp.399-441.

23. Asanuma T. and Obotaka T., 1979, "Gas velocity measurements of a motored and firing engine by Laser anemometry", SAE paper 790096, pp. 401- 409.

Table I Engine configuration details

Engine Make, Model	Kirloskar, RB-33 coupled to a 25kVA alternator
Rated output (in diesel)	28 kW @ 1500 RPM
Output measured (in diesel)*	24 kW (21kWe) @ 1500 RPM
Bore x Stroke	110 x 116 mm
Number of cylinder	3
Type of cooling	Water
Compression ratio	17:1
Bumping clearance	1.5 mm
Combustion chamber	Flat cylinder head and Bowl-in piston type
Squish area	70%
Ignition system	Battery based distributor type with ignition advance/retard facility
Spark plug type & location	Cold, offset from centre of combustion chamber by 8mm
Valve port	Tangential –directed type
Valve timing	Inlet valve opening – 26 BTDC Inlet valve closing – 66 ATDC Exhaust valve opening – 64 BBDC Exhaust valve closing – 38 ATDC
Alternator Efficiency#	87%
Gasification Efficiency$	80%

* At Bangalore, 1000 m above sea level;
# As per manufacturer's specifications;
$ Reference

Table 2 Summary of 0-D predictions (Pre-TC & Post-TC) at varying CR and ignition advance using turbulence intensity results from CFD analysis and experimental results on an engine with similar configuration [18]. The flame shape and the propagation speeds accounted in the prediction both inside and outside the bowl is also given

Case	Ignition advance before TC (° CA)		Flame shape; Propagation speed		Turbulence intensity obtained from		Quality of 0-D Prediction	
	CR 17.0	CR 11.5	Inside bowl	Outside bowl	Pre-TC	Post-TC	Pre-TC	Post-TC
I	26	-	Spherical; Normal	Spherical; Normal	CFD CFD	CFD Expt {18]	Good Good	Lower Good
II	22	-	Spherical; Normal	Spherical; Normal	CFD CFD	CFD Expt [18]	Good Good	Lower Good
III	-	27	Spherical; Normal	Spherical; Normal	CFD CFD	CFD Expt [18]	Good Good	Lower Good
IV	17	-	Spherical; Normal Spherical; Normal	Spherical; Normal Flat; Enhanced	CFD	Expt[18]	Good Good	Lower Good
V	-	17	Spherical; Normal Spherical; Normal	Spherical; Normal Flat; Enhanced	CFD	Expt [18]	Good Good	Lower Higher
VI	12	-	Spherical; Normal	Flat; Enhanced	CFD	Expt [18]	Good	Lower
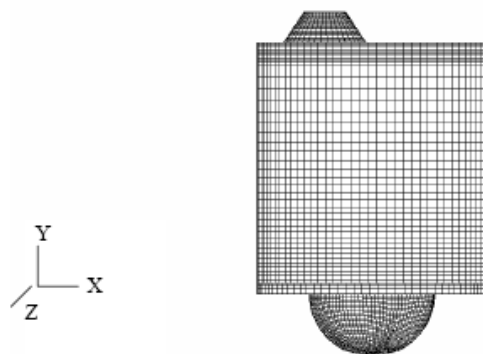
Fig. 1 Grid arrangement with the intake valve fully open and piston at bottom centre used for CFD calculations.
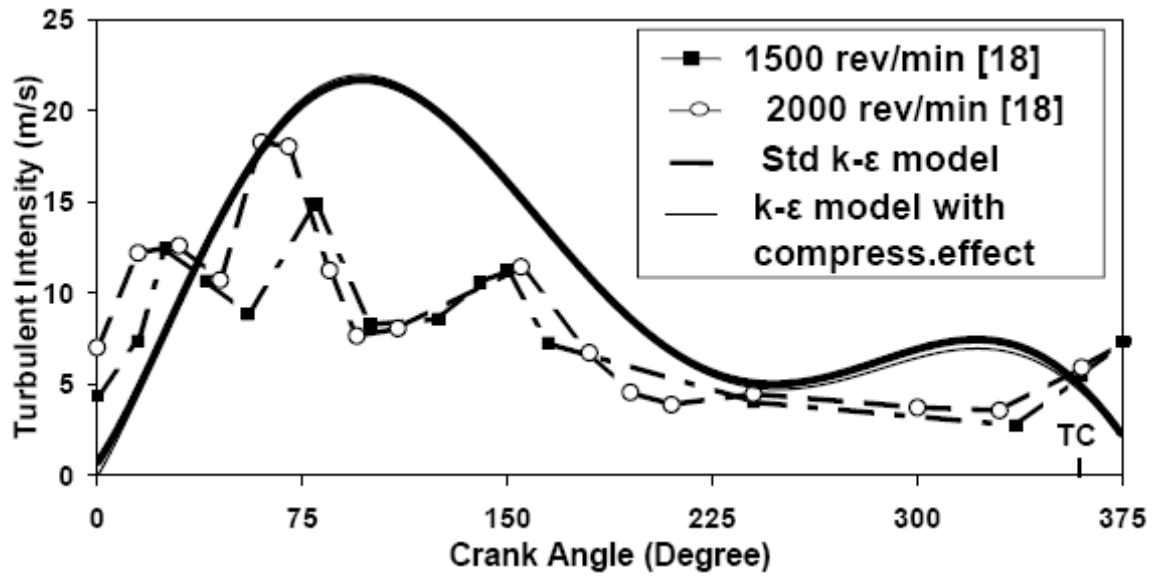
Fig. 2. Comparison of CFD results using k-ε model (with and without compressibility effect) against experimental result of similar configuration engine [18].
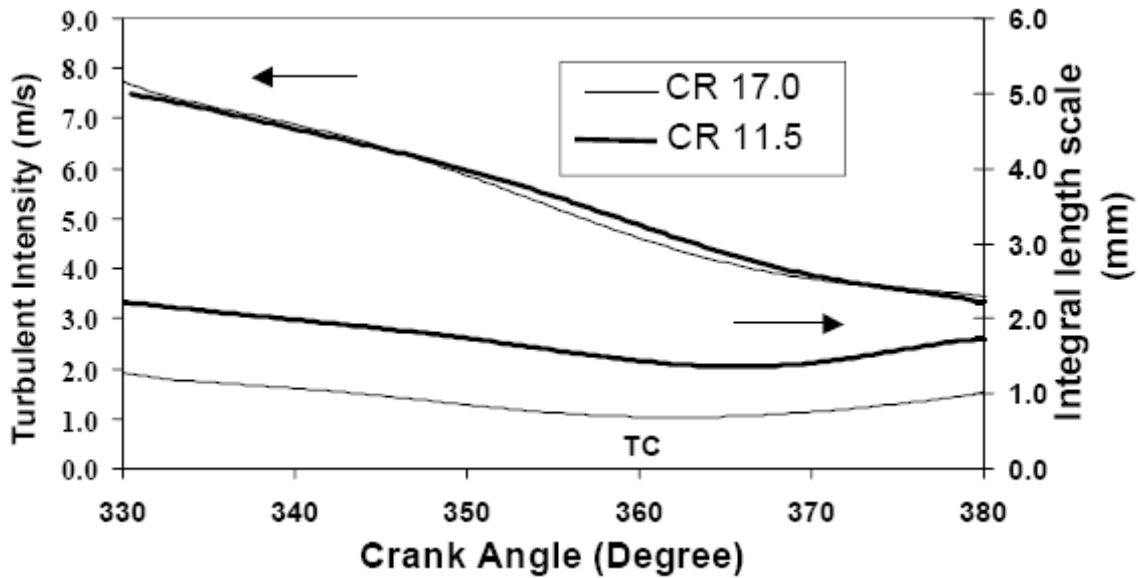
Fig. 3. Comparison of turbulence intensity and length scale using standard k-ε at varying CR.
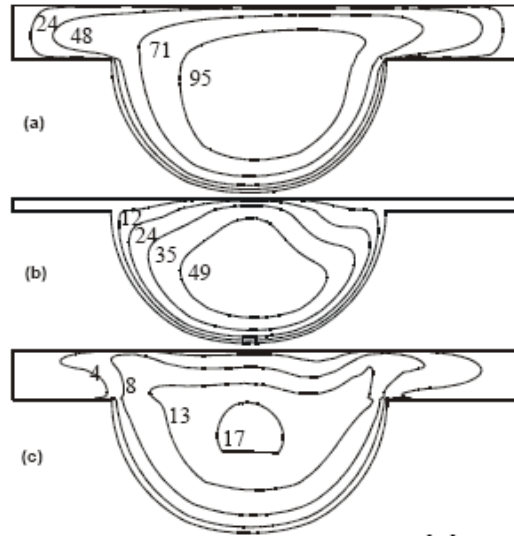
Fig. 4 CFD results: Contour plot of turbulence kinetic energy (m2/s2) on a vertical plane through the centre of the geometry (a) 30° CA before TC (b) TC @ 360° CA (c) 30° CA after TC.
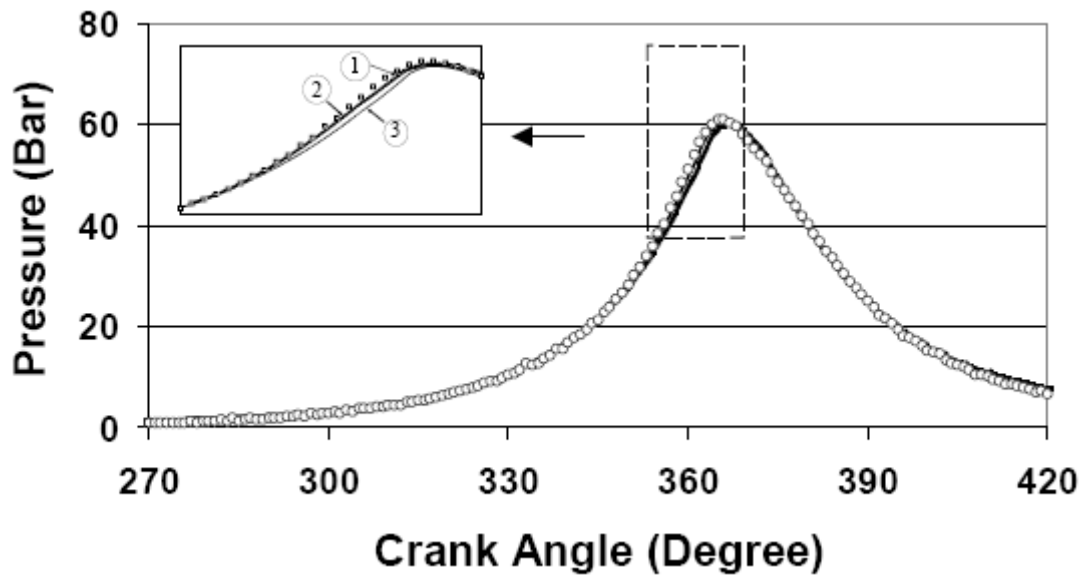
Fig. 5 Comparison of 0-D predictions with experimental p-θ results for CR =17 at an ignition advance of 260 before TC. Circle indicates experimental values (ensemble averaged over 30 consecutive cycles). Solid lines indicate 0-D predictions. Inset shows predictions with the following trends for u' (1) CFD result in pre-TC period and [18] trend in post-TC (2) CFD results in pre-TC and post-TC period. (3) Trend in pre-TC and post-TC period using [18].
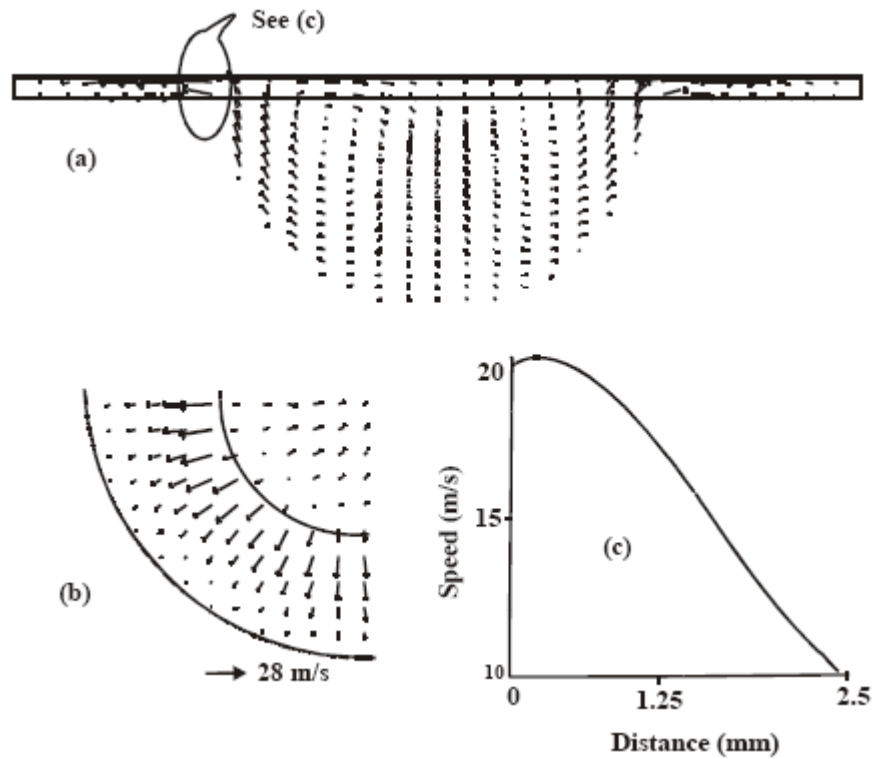
Fig. 6 CFD results: Velocity vectors during reverse squish at 10° CA after TC (a) vertical plane through centre of the geometry – notice the flow vectors pointed outwards. (b) One quarter image in the horizontal plane at a distance of 1mm below the cylinder head. Dotted line indicates the outer periphery of the bowl -notice higher gas velocities in the flat region (c) gas speed measuring from cylinder head towards piston top – close to the outer periphery of the bowl.
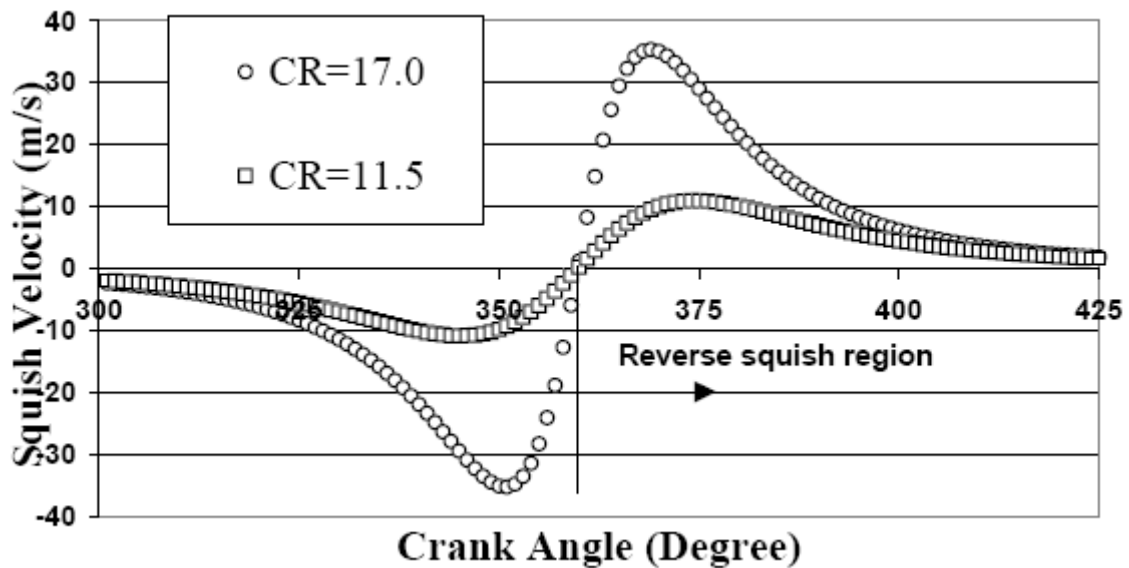
Fig. 7 Squish velocity (omitting effects like gas inertia, friction, gas leakage past piston rings, heat transfer) in the absence of combustion during reverse squish period at different CR using empirical correlation [7].
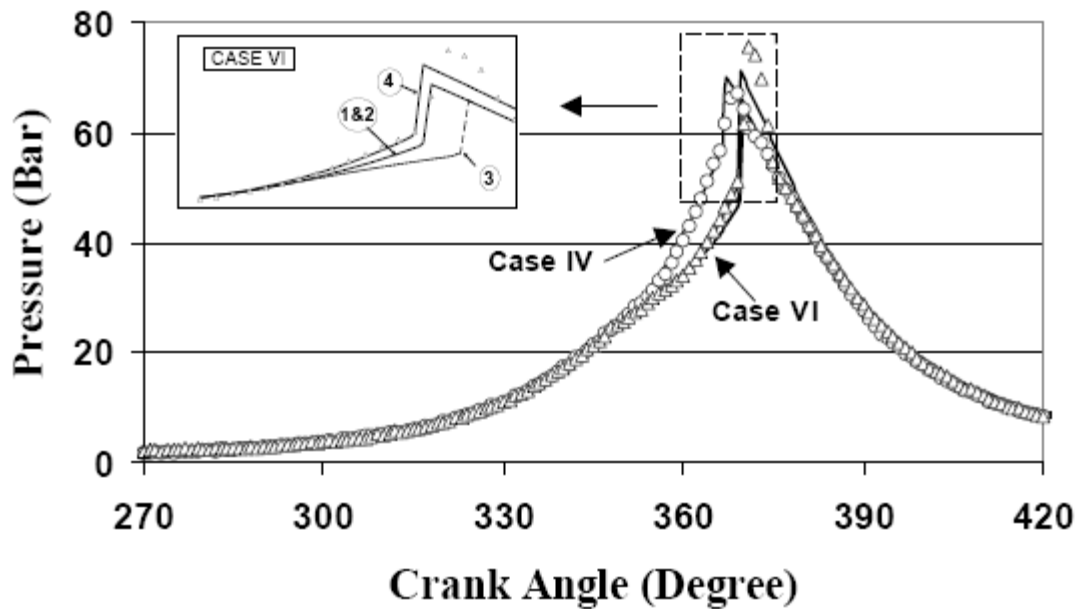
Fig. 8 Comparison of 0-D predictions with experimental results at CR =17. Circle and Triangle indicate experimental values (ensemble averaged over 30 consecutive cycles) at 17° and 12°CA ignition advance respectively. Solid lines indicate 0-D predictions. Inset shows predictions (at 12° CA ignition advance) with the following trends for u (1) CFD result in pre-TC period and [18] trend in post-TC – {1} (2) trend in pre-TC and post-TC period using [18] (3) CFD results in pre-TC and post-TC period. (4) same as {1} along with methane higher by 4% - which implies increase in energy content of the mixture by 6.5%.